Effect of radiation damping on the spectral response of plasmonic components

Mikhail A. Kats,[1] Nanfang Yu,[1] Patrice Genevet,[1,2] Zeno Gaburro,[1,3] and Federico Capasso[1,*]

[1]*School of Engineering and Applied Sciences, Harvard University, Cambridge, Massachusetts 02138, USA*
[2]*Institute for Quantum Studies and Dept. of Physics, Texas A&M University, College Station, Texas, 77843, USA*
[3]*Dipartimento di Fisica, Università degli Studi di Trento, via Sommarive 14,38100 Trento, Italy*
**capasso@seas.harvard.edu*

Abstract: We explore the relationship between the near-field enhancement, absorption, and scattering spectra of localized plasmonic elements. A simple oscillator model including both internal and radiative damping is developed, and is shown to accurately capture the near- and far-field spectral features of linear optical antennas, including their phase response. At wavelengths away from the interband transitions of the metal, we expect the absorption of a plasmonic element to be red-shifted relative to the scattering, and the near-field to be red-shifted relative to both.

©2011 Optical Society of America

OCIS codes: (250.5403) Plasmonics; (230.4910) Oscillators.

References and links

1. S. Lal, S. Link, and N. J. Halas, "Nano-optics from sensing to waveguiding," Nat. Photonics **1**(11), 641–648 (2007).
2. H. A. Atwater, "The promise of plasmonics," Sci. Am. **296**(4), 56–63 (2007).
3. M. Pelton, J. Aizpurua, and G. Bryant, "Metal-nanoparticle plasmonics," Laser Photonics Rev. **2**, 3 (2008).
4. E. Cubukcu, N. Yu, E. J. Smythe, L. Diehl, K. B. Crozier, and F. Capasso, "Plasmonic laser antennas and related devices," IEEE J. Sel. Top. Quantum Electron. **14**(6), 1448–1461 (2008).
5. S. A. Maier, *Plasmonics: fundamentals and applications* (Springer-Verlag, New York, 2007)
6. L. Novotny and N. van Hulst, "Antennas for light," Nat. Photonics **5**, 83–90 (2011).
7. K. A. Willets and R. P. Van Duyne, "Localized surface plasmon resonance spectroscopy and sensing," Annu. Rev. Phys. Chem. **58**, 267–297 (2006).
8. S. Nie and S. R. Emory, "Probing single molecules and single nanoparticles by surface-enhanced Raman scattering," Science **275**, 1102–1106 (1997).
9. M. Osawa, "Surface-enhanced infrared absorption," Top. Appl. Phys. **81**, 163–187 (2001).
10. R. Adato, A. A. Yanik, J. J. Amsden, D. L. Kaplan, F. G. Omenetto, M. K. Hong, S. Erramilli, and H. Altug, "Ultra-sensitive vibrational spectroscopy of protein monolayers with plasmonic nanoantenna arrays," Proc. Natl. Acad. Sci. U.S.A. **106**, 46 (2009).
11. J. Renger, R. Quidant, N. van Hulst, and L. Novotny, "Surface-enhanced nonlinear four-wave mixing," Phys. Rev. Lett. **104**(4), 046803 (2010).
12. P. Genevet, J. P. Tetienne, E. Gatzogiannis, R. Blanchard, M. A. Kats, M. O. Scully, and F. Capasso, "Large enhancement of nonlinear optical phenomena by plasmonic nanocavity gratings," Nano Lett. **10**(12), 4880–4883 (2010).
13. L. R. Hirsch, R. J. Stafford, J. A. Bankson, S. R. Sershen, B. Rivera, R. E. Price, J. D. Hazle, N. J. Halas, and J. L. West, "Nanoshell-mediated near-infrared thermal therapy of tumors under magnetic resonance guidance," Proc. Natl. Acad. Sci. U.S.A. **100**, 23 (2003).
14. T. Kosako, Y. Kadoya, and H. F. Hofmann, "Directional control of light by a nano-optical Yagi-Uda antenna," Nat. Photonics **4**(5), 312–315 (2010).
15. M. W. Knight, H. Sobhani, P. Nordlander, and N. J. Halas, "Photodetection with active optical antennas," Science **332**(6030), 702–704 (2011).
16. N. Yu and F. Capasso, "Wavefront engineering for mid-infrared and terahertz quantum cascade lasers," J. Opt. Soc. Am. B **27**(11), B18 (2010).
17. N. Yu, P. Genevet, M. A. Kats, F. Aieta, J. P. Tetienne, F. Capasso, and Z. Gaburro, "Light propagation with phase discontinuities: generalized laws of reflection and refraction," Science Express **10**, 1210713 (2011).
18. K. L. Kelly, E. Coronado, L. L. Zhao, and G. C. Schatz, "The optical properties of metal nanoparticles: the influence of size, shape, and dielectric environment," J. Phys. Chem. B **107**(3), 668–677 (2003).

#154838 - $15.00 USD Received 20 Sep 2011; revised 2 Oct 2011; accepted 2 Oct 2011; published 19 Oct 2011
(C) 2011 OSA

19. N. K. Grady, N. J. Halas, and P. Nordlander, "Influence of dielectric function properties on the optical response of plasmon resonant metallic nanoparticles," Chem. Phys. Lett. **399**(1-3), 167–171 (2004).
20. S. Bruzzone, M. Malvaldi, G. P. Arrighini, and C. Guidotti, "Light scattering by gold nanoparticles: role of simple dielectric models," J. Phys. Chem. B **108**(30), 10853–10858 (2004).
21. A.-S. Grimault, A. Vial, and M. Lamy de la Chapelle, "Modeling of regular gold nanostructures arrays for SERS applications using a 3D FDTD method," Appl. Phys. B **84**(1-2), 111–115 (2006).
22. G. W. Bryant, F. J. García de Abajo, and J. Aizpurua, "Mapping the plasmon resonances of metallic nanoantennas," Nano Lett. **8**(2), 631–636 (2008).
23. B. M. Ross and L. P. Lee, "Comparison of near- and far-field measures for plasmon resonance of metallic nanoparticles," Opt. Lett. **34**(7), 896 (2009).
24. J. Zuloaga and P. Nordlander, "On the energy shift between near-field and far-field peak intensities in localized plasmon systems," Nano Lett. **11**(3), 1280–1283 (2011).
25. S. Zhang, D. A. Genov, Y. Wang, M. Liu, and X. Zhang, "Plasmon-induced transparency in metamaterials," Phys. Rev. Lett. **101**(4), 047401 (2008).
26. N. Liu, L. Langguth, T. Weiss, J. Kästel, M. Fleischhauer, T. Pfau, and H. Giessen, "Plasmonic analogue of electromagnetically induced transparency at the Drude damping limit," Nat. Mater. **8**(9), 758–762 (2009).
27. D. J. Griffiths, *Introduction to Electrodynamics, 3rd ed.* (Benjamin Cummings, 1999)
28. W. Heitler, *The Quantum Theory of Radiation, 3rd ed.* (Oxford Univ. Press, London, 1954)
29. J. Ginn, D. Shelton, P. Krenz, B. Lail, and G. Boreman, "Polarized infrared emission using frequency selective surfaces," Opt. Express **18**(5), 4557–4563 (2010).
30. N. Yu, E. Cubukcu, L. Diehl, M. A. Belkin, K. B. Crozier, F. Capasso, D. Bour, S. Corzine, and G. Hofler, "Plasmonic quantum cascade laser antenna," Appl. Phys. Lett. **91**(17), 173113 (2007).
31. Our FDTD simulations were performed with Lumerical FDTD Solutions 6.5.
32. E. D. Palik, Handbook of Optical Constants of Solids Vol. 3, (Academic Press, 1997)
33. N. W. Ashcroft and N. D. Mermin, *Solid State Physics* (Thomson, 1976).
34. H. M. van Driel, "Optical effective mass of high density carriers in silicon," Appl. Phys. Lett. **44**(6), 617 (1984).
35. M. M. Alvarez, J. T. Khoury, T. G. Schaaff, M. N. Shafigullin, I. Vezmar, and R. L. Whetten, "Optical absorption spectra of nanocrystal gold molecules," J. Phys. Chem. B **101**(19), 3706–3712 (1997).
36. S. J. Oldenburg, G. D. Hale, J. B. Jackson, and N. J. Halas, "Light scattering from dipole and quadrupole nanoshell antennas," Appl. Phys. Lett. **75**(8), 1063 (1999).

1. Introduction

Plasmonic elements such as metallic nanoparticles and optical antennas have recently emerged as an effective technology for confining and controlling light at the nanoscale [1–6]. Localized surface plasmon resonances (LSPRs) are responsible for the strong interaction between light and metallic nanostructures, and have enabled a number of near-field applications such as LSPR sensing [7], surface-enhanced Raman scattering (SERS) spectroscopy [8], surface-enhanced infrared absorption (SEIRA) spectroscopy [9, 10], enhanced nonlinear wave mixing [11, 12], and even nanoparticle-based cancer therapy [13], as well as far-field applications like emission engineering [14], frequency-sensitive photodetectors [15], wavefront engineering of semiconductor lasers [16], and molding light propagation at engineered interfaces [17].

In the study of localized surface plasmon systems, a number of both near- and far-field quantities are used to characterize plasmonic resonances with the most common ones being near-field enhancement, and the absorption and scattering cross-sections (the last two are often combined into an extinction cross-section). It has been observed that the wavelength dependence of near-field quantities such as electric field enhancement can be significantly red-shifted compared with far field quantities such as scattering [18–23]. This discrepancy has significant implications for plasmonic applications where care must be taken to optimize the appropriate figure of merit for the wavelength of interest.

Recently, Zuloaga et al proposed that this shift can be understood as a general consequence of the behavior of damped, driven harmonic oscillators, in which the maximum oscillation amplitude is at a lower frequency than the peak absorption [24]. Zuloaga et al relate the oscillation amplitude to the plasmon-induced near fields and the oscillator absorption to the extinction cross-section. Similar models involving a charge on a spring have been used in the past to describe the plasmonic analogue of electromagnetically induced transparency (EIT), in which a dipole antenna element (modeled as a damped, driven

#154838 - $15.00 USD Received 20 Sep 2011; revised 2 Oct 2011; accepted 2 Oct 2011; published 19 Oct 2011
(C) 2011 OSA

oscillator) was coupled to a dark quadrupole antenna (a damped, undriven oscillator) via near-field interactions [25, 26].

In aforementioned simple models for LSPRs, all damping mechanisms were combined into a single loss term proportional to the charge velocity, as in damped harmonic oscillators. However, LSPR modes actually decay via two distinct channels: internal damping via free carrier absorption and emission of light into free space which we recognize as scattering. In this report, we explicitly account for these two decay channels and show that in LSPR systems the near-field, absorption, and scattering spectra are all expected to peak at different frequencies and have distinct profiles. We find excellent agreement between our model and electromagnetic simulations of plasmonic antennas in the infrared spectral range.

2. Model

We begin by analyzing a system in which a charge q located at $x(t)$ with mass m on a spring with spring constant κ (Fig. 1(a)) is driven by an harmonic incident electric field with frequency ω, and experiences internal damping with damping coefficient Γ_a:

$$m\frac{d^2x}{dt^2}+\Gamma_a\frac{dx}{dt}+\kappa x = qE_0e^{i\omega t}+\Gamma_s\frac{d^3x}{dt^3} \tag{1}$$

In addition to the internal damping force $\Gamma_a\, dx/dt$, the charge experiences an additional force $\Gamma d^3x/dt^3$ due to radiation reaction, where $\Gamma_s = q^2/6\pi\epsilon_0c^3$. This term describes the recoil that the charge feels when it emits radiation, and is referred to as the Abraham-Lorentz force or the radiation reaction force [27]. Since classical laws of electrodynamics necessitate that an accelerating charge release energy in the form of radiation, conservation of energy implies that this charge must consequently lose kinetic energy. The form of the radiation reaction force can be derived by applying an energy balance argument to the classical Larmor formula for radiated power, and it can also be seen as the force which the field produced by the charge exerts on the charge itself [28].

For our charge-on-a-spring model, the radiation reaction term has to be included for physical consistency, and cannot be absorbed into the internal damping coefficient Γ_a while maintaining its frequency-independence.

By assuming harmonic motion $x(\omega,t) = x_0e^{i\omega t}$ we can immediately write down the steady-state solution to Eq. (1) as

$$x(\omega,t) = \frac{(q/m)E_0}{(\omega_0^2-\omega^2)+i\frac{\omega}{m}(\Gamma_a+\omega^2\Gamma_s)}e^{i\omega t} = x_0(\omega)e^{i\omega t} \tag{2}$$

where $x_0(\omega)$ contains the amplitude and phase response of the oscillator and $\omega_0 = \sqrt{k/m}$.

Time-averaged power dissipated by an oscillator can be written as $P(\omega) = F(\omega)^*(i\omega x_0(\omega))$ where $F(\omega)^*$ is the complex conjugate of the applied force. Therefore, by using Eqs. (1)-(2), we can write down the expressions for the absorbed and scattered power by the oscillator as:

$$\begin{aligned} P_{abs}(\omega) &= \omega^2\Gamma_a\left|x_0(\omega)\right|^2 \\ P_{scat}(\omega) &= \omega^4\Gamma_s\left|x_0(\omega)\right|^2 \end{aligned} \tag{3}$$

where $\left|x_0(\omega)\right|^2$ is the magnitude-squared of the oscillation amplitude which can be written as

#154838 - $15.00 USD Received 20 Sep 2011; revised 2 Oct 2011; accepted 2 Oct 2011; published 19 Oct 2011
(C) 2011 OSA

$$\left|x_0(\omega)\right|^2 = \frac{(q/m)^2 E_0^{\,2}}{(\omega_0^{\,2} - \omega^2)^2 + \frac{\omega^2}{m^2}(\Gamma_a + \omega^2 \Gamma_s)^2}. \tag{4}$$

The value $x_0(\omega)$ is in general a complex quantity, and related to the frequency-dependent phase $\phi(\omega)$ by $x_0(\omega) = \left|x_0(\omega)\right| e^{i\phi(\omega)}$.

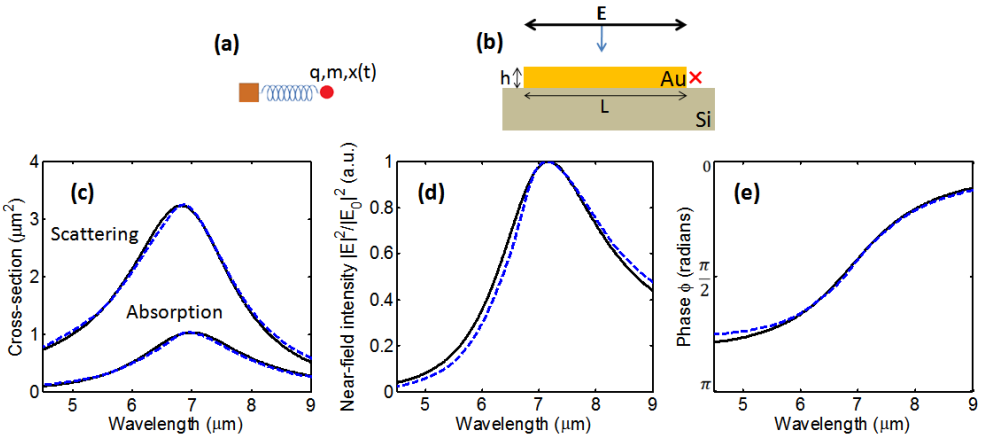

Fig. 1. (a) Representation of an optical antenna in oscillator form, where q is the charge, m is the inertial mass, and x(t) is the displacement from the equilibrium position. (b) Schematic of a gold optical antenna (length L = 1μm, height h = 50nm, width w = 130nm) on a silicon substrate, illuminated by a normally incident plane wave polarized along the antenna axis. The cross represents the point ~4 nm away from the antenna edge where the near-field is calculated. (c) Scattering and absorption cross-sections as calculated via FDTD (dashed lines) and the model (solid lines). (d) Near-field intensity enhancement calculated by the model (solid line) and via FDTD (dashed line) at the location identified by the cross, with the incident field subtracted off. (e) Oscillator phase (which also represents the phase of the near-field).

3. Interpretation

LSPR systems are examples of harmonic oscillators [17, 24, 29], and simple charge-on-a-spring oscillator models with a single damping term have previously been utilized to gain physical understanding of complex plasmonic systems [25, 26].

Our extended oscillator model can shed light on the relationship between the near-field, absorption, and scattering spectra in plasmonic elements. We expect our explicit inclusion of the radiative damping term to provide additional physical insight compared to the aforementioned models: this term makes the model physically consistent, and is reminiscent of the radiative damping corrections that have been made to improve the analytical analysis of metallic spheroids via the modified long-wavelength approximation (MLWA) [18].

As a representative LSPR system, we consider a gold linear plasmonic antenna on a silicon substrate designed to resonate in the mid-infrared spectral range (Fig. 1(b)). Such antennas have found uses in focusing light from quantum cascade lasers [30], SEIRA spectroscopy [10], and infrared photodetectors [15]. We specifically consider LSPR resonators at wavelengths much longer than those corresponding to interband transitions in gold to isolate the resonant nature of the antennas from the material resonances.

If we interpret our plasmonic antenna as an oscillator that obeys Eqs. (1)-(4), we can define the absorption and scattering cross-sections $C_{abs}(\omega) = P_{abs}(\omega)/I_0$ and $C_{scat}(\omega) = P_{scat}(\omega)/I_0$, where I_0 is the incident intensity, which are measures of how much of the incident power the oscillator is able to absorb or scatter. Furthermore, we can calculate the near-field intensity enhancement at the tip of the antenna as

#154838 - $15.00 USD Received 20 Sep 2011; revised 2 Oct 2011; accepted 2 Oct 2011; published 19 Oct 2011
(C) 2011 OSA

$|E_{near}(\omega)|^2 \propto |x_0(\omega)|^2$ since the plasmon-induced near-field is directly proportional to the charge density accumulating at the edges of the antenna [24].

By examining Eqs. (3)-(4) and noting that $P_{scat} \propto \omega^2 P_{abs} \propto \omega^4 |E_{near}(\omega)|^2$ we can deduce that the scattering spectrum $P_{scat}(\omega)$ will be blue-shifted relative to the absorption spectrum $P_{abs}(\omega)$, which will in turn be blue-shifted relative to the near-field intensity enhancement spectrum $|E_{near}(\omega)|^2$. These spectral differences can be clearly seen in finite difference time domain (FDTD) simulations of gold linear antennas [31] in which we used the complex permittivity data for gold from Palik [32]. In Fig. 1(c-e), we show the scattering and absorption cross-sections, the near-field intensity at the edge, and the near-field phase, respectively, for our antenna as calculated by FDTD (dashed lines). We fit the simulation results presented in Fig. 1(c) with Eqs. (3) to obtain the parameters q, m, ω_0, and Γ_a.

The parameters obtained from the fit are consistent with the interpretation that the driving and radiative damping of the antenna mode are due to conduction electrons in the gold comprising the antenna. Assuming a carrier density of 5.9 x 10^{22} cm^{-3} in gold [33] and volume V = 6.5 x 10^{-15} cm^3 for the antenna in Fig. 1, we expect ~3.8 x 10^8 free electrons to be present in the antenna. A Drude model fit to the mid-IR data for gold in Palik [32] yields a plasma frequency of $\omega_p \sim 1.2 \times 16\, s^{-1}$, which suggests an electron optical effective mass $m_e^* \sim 1.35 m_e$ (as defined in [34]) where m_e is the free electron mass. On the other hand, the parameters q and m from our fit correspond to ~2.3 x 10^8 electrons of effective mass $m_e^* \sim 1.5 m_e$, close to the values obtained from the carrier density in gold and the antenna volume. The total charge participating appears to be ~60% of the combined charge of the conduction electrons in the antenna, which is consistent with the fact that not all of the electrons interact equally with the driving and the scattered fields due to the skin depth effect.

The resulting model is able to explain the peak spectral position and general shape of the near-field intensity (Fig. 1(d)), as well as the phase response of the antenna (Fig. 1(e)). Note that no additional fitting was done to obtain the near-field curves in Fig. 1(d, e). This result suggests that this model can predict the near-field amplitude and phase response from experimental far-field spectra of antennas, which are much easier to obtain than near-field measurements.

To further illustrate the spectral differences between our quantities of interest, in Fig. 2 we plot the wavelength peaks of the scattering (blue), absorption (red), and near-field (black) spectra for antenna lengths from 0.5 μm to 1.5 μm both on a silicon substrate (solid lines) and embedded in silicon (dashed lines). In both cases, the aforementioned trend remains unchanged, with the near-field peak always red-shifted relative to the absorption, and with both red-shifted relative to the scattering spectrum.

#154838 - $15.00 USD Received 20 Sep 2011; revised 2 Oct 2011; accepted 2 Oct 2011; published 19 Oct 2011
(C) 2011 OSA

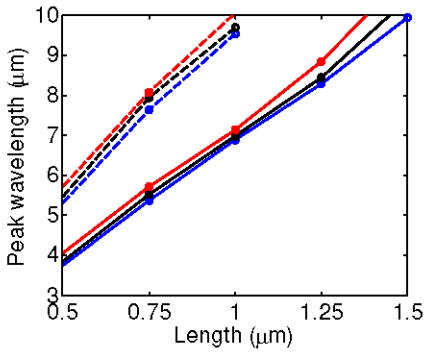

Fig. 2. Peak wavelengths of the near-field (red), absorption (black), and scattering (blue) of linear antennas (w = 130nm, h = 50nm, gold) of various lengths sitting on (solid lines) and embedded in (dashed lines) a silicon substrate

It is important to note that our results remain valid only for wavelengths far enough away from any material resonances. For example, in the visible range near an interband transition for gold [35] the absorption spectrum for nanospheres peaks at a lower wavelength than the scattering spectrum [23], contrary to the predictions of our model. It appears that our model can be safely applied to noble metal structures in the near- and mid-infrared spectral range and longer wavelengths; for example see Oldenburg et al in which the scattering spectra of near-infrared dipolar, quadrupolar, and octupolar modes in nanoshells have been shown to all be blue-shifted relative to the absorption spectra [36]. To treat the short wavelength regime our model could be augmented by introducing an additional oscillator with a coupling term to represent the resonant response of the material; in fact, a Lorentz oscillator model is often used to account for this well-known effect of bound electrons in metals when calculating its complex permittivity [5] [35].

3. Conclusion

In this report, utilized a simple oscillator model with an explicit radiation damping term to explain the differences in the near-field, absorption, and scattering spectra of localized plasmonic systems away from material resonances. We fit our model to full-wave numerical simulations of the scattering and absorption cross-sections of plasmonic antennas in the infrared, which enabled us to predict the near-field amplitude and phase response with high fidelity. The resulting fits yielded parameters that were consistent with the interpretation that the interaction of the incident and scattered fields with the antenna is via the combined mass and charge of the conduction electrons in the metal.

Our model can shed light on the behavior of plasmonic systems without resorting to elaborate theories or numerical approaches. This understanding will be beneficial for the design of plasmonic elements for near- and far-field applications.

Acknowledgments

This work was supported in part by the Defense Advanced Research Projects Agency (DARPA) N/MEMS S&T Fundamentals program under grant no. N66001-10-1-4008 issued by the Space and Naval Warfare Systems Center Pacific (SPAWAR). M. A. Kats is supported by the National Science Foundation through a Graduate Research Fellowship. P. Genevet acknowledges support from the Robert A. Welch Foundation (A-1261). Z. Gaburro acknowledges funding from the European Communities Seventh Framework Programme (FP7/2007-2013) under grant agreement PIOF-GA-2009-235860. We thank Romain Blanchard, Francesco Aieta, Jonathan Fan, Ken Crozier, and Alexey Belyanin for helpful discussions.

#154838 - $15.00 USD Received 20 Sep 2011; revised 2 Oct 2011; accepted 2 Oct 2011; published 19 Oct 2011
(C) 2011 OSA